

Very High Energy γ -rays from e^\pm Pair Halos

A. Eungwanichayapant

*School of Science, Mae Fah Luang University, 333 Ta-Sud
Muang, Chiang Rai, 57100, Thailand
anant.e@gmail.com*

F. Aharonian

*Dublin Institute for Advanced Studies, 31 Fitzwilliam Place, Dublin 2, Ireland and
Max-Planck-Institut für Kernphysik, Saupfercheckweg 1
69117 Heidelberg, Germany
Felix.Aharonian@mpi-hd.mpg.de*

Received Day Month Year

Revised Day Month Year

In this paper we study the formation of giant electrons-positron pair halos around the powerful high energy extragalactic sources. We investigate the dependence of radiation of pair halos, in particular the spectral and angular distributions on the energy spectrum of the primary gamma-rays, the redshift of the source, and the flux of the extragalactic background light.

Keywords: Very High Energy γ -rays, electromagnetic cascade

1. Introduction

Interactions of very high energy (VHE) gamma-rays with the diffuse Extragalactic Background light (EBL)^{1,2}, as well as the the possible effects caused by propagation of secondary (pair-produced) electrons in the intergalactic medium (see e.g. Ref. 3), make the high energy gamma-rays unique carries of cosmological information about the epochs of formation of galaxies and their evolution in the past (see e.g. Ref. 4, 5, 6, 7, 8, 9). The method is based on the distinct features in the spectra of high energy gamma-rays arriving from distant extragalactic objects caused by interactions with EBL.

A serious obstacle in practical realization of this method is our poor knowledge concerning the primary (intrinsic) gamma-ray spectra produced in the source¹⁰. It is believed that the well coordinated observations of gamma-ray blazars in different energy bands should allow gamma-ray astronomers to identify the radiation mechanisms, derive the principal model parameters, and thus reconstruct the intrinsic gamma-ray spectra based on spectral and temporal properties of blazars (see e.g. Ref. 11). Even so, for reliable estimates of the intergalactic absorption effect, and ultimately for derivation of the flux and spectrum of EBL, one should take into

2 *A. Eungwanichayapant and F.A. Aharonian*

account possible integral absorption of gamma-rays. The importance of the internal photon-photon absorption in blazars has been discussed by many authors, in particular just after the discovery by COS B of the first gamma-ray blazar - 3C273¹². The complex behavior of internal photon-photon absorption may result in a rather "irregular" deformation of the spectrum of primary gamma-rays (from *steepening* or even sharp cutoffs to *hardening*)¹³. This, as well as the effects related to the redshift of blazars¹⁴, challenge the feasibility of reliable derivation of EBL based on absorption features in the gamma-ray spectra of extragalactic objects.

Moreover, strictly speaking, the intergalactic absorption features contain information about the product of the diffuse extragalactic background radiation density w_r and the Hubble constant H_0 . Fortunately, it is possible to decouple w_r and H_0 by studying the spectral and angular characteristics of VHE γ radiation from hypothetical electron-positron pair halos surrounding powerful nonthermal extragalactic objects. These giant structures are unavoidably formed around any extragalactic VHE source due to development of pair cascades initiated by interactions of primary multi-TeV photons with EBL¹⁵.

2. Basic processes of formation of pair halos

For formation of electron-positron pair halos around extragalactic objects, the photon-photon pair production (PP) and inverse Compton scattering (IC) are two principal processes which initiate and support the electromagnetic cascade development¹⁵. The mean free pathlengths and the energy spectra of secondary particles produced at these interactions are described below.

2.1. Pair production

For the pair production at a collision of a gamma-ray photon of energy ε with a target photon of energy ω the following threshold conditions is required:

$$2(1 - \beta'^2)^{-1} = \varepsilon\omega(1 - \cos\theta), \quad (1)$$

where β' is a velocity of the electron (positron) e^\pm in the CM frame and θ is an angle between the momenta of two photons in lab frame (below we will use the energy of e^\pm pairs in units of the electron rest mass, $m_e c^2$).

The mean free path length Λ_{PP} of a gamma-ray of energy ε traveling through the isotropically-distributed photon gas of differential energy density $n(\omega)$ is

$$\Lambda_{PP}^{-1}(\varepsilon) = \int_{\omega_{th}}^{\infty} \bar{\sigma}_{PP} n(\omega) d\omega, \quad (2)$$

where $\bar{\sigma}$ is the cross-section averaged over directions of interacting photons:

$$\bar{\sigma}_{PP} = \frac{1}{2} \int_{-1}^{1-2/s_0} (1 - \mu) \sigma_{PP} d\mu. \quad (3)$$

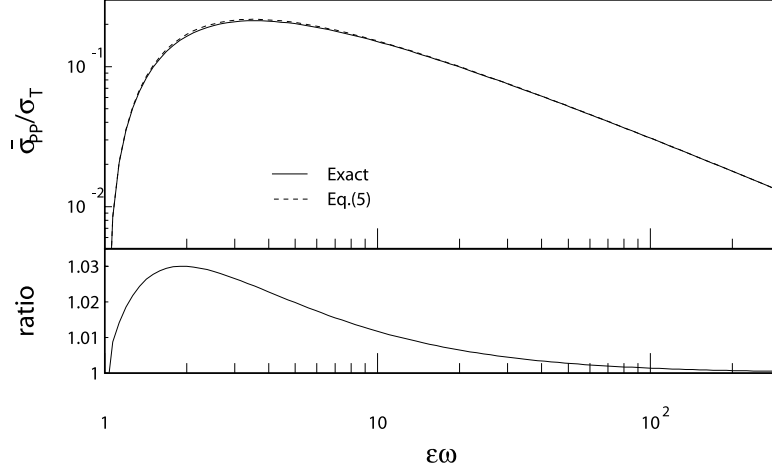


Fig. 1. Top panel: The cross section of photon-photon pair production $\bar{\sigma}_{PP}$ (in units of the Thomson cross section σ_T) calculated using the exact expression (solid line) and the approximation given by Eq.(5) (dashed line). Bottom panel: the ratio of these two presentations of the cross-section.

Here $s_0 = \epsilon\omega$, $\mu = \cos\theta$ and σ_{PP} is the total cross section of the process (see e.g. Ref. 16)

$$\sigma_{PP} = \frac{3}{16}\sigma_T(1 - \beta'^2)\beta' \left[\frac{(3 - \beta'^4)}{\beta'} \ln \frac{1 + \beta'}{1 - \beta'} + \frac{1}{2}(\beta'^2 - 2) \right], \quad (4)$$

where σ_T is the Thomson cross section. For integration of Eq.(3) we use the following approximation¹⁷,

$$\begin{aligned} \bar{\sigma}_{PP} = \frac{3\sigma_T}{2s_0^2} & \left[\left(s_0 + \frac{1}{2} \ln s_0 - \frac{1}{6} + \frac{1}{2s_0} \right) \times \ln(\sqrt{s_0} + \sqrt{s_0 - 1}) \right. \\ & \left. - \left(s_0 + \frac{4}{9} - \frac{1}{9s_0} \right) \sqrt{1 - \frac{1}{s_0}} \right], \end{aligned} \quad (5)$$

which provides an accuracy better than 3% as demonstrated in Fig.1.

The resulting e^\pm energy distribution is described as¹⁸

$$\begin{aligned} \frac{dN_{e^\pm}(\gamma, \omega, \epsilon)}{d\gamma} = \frac{3\sigma_T}{32\omega^2\epsilon^3} & \left[\frac{4\epsilon^2}{(\epsilon - \gamma)\gamma} \times \ln \frac{4\omega(\epsilon - \gamma)\gamma}{\epsilon} - 8\omega\epsilon \right. \\ & \left. + \frac{2(2\omega\epsilon - 1)\epsilon^2}{(\epsilon - \gamma)\gamma} - \left(1 - \frac{1}{\omega\epsilon} \right) \frac{\epsilon^4}{(\epsilon - \gamma)^2\gamma^2} \right], \end{aligned} \quad (6)$$

where γ is the energy of the electron (positron) (in $m_e c^2$ units) and $\epsilon = \epsilon + \omega \approx \epsilon$ is the photon energy in the lab-frame. The range of γ is

$$\frac{\epsilon}{2} \left(1 - \sqrt{1 - \frac{1}{\epsilon\omega}} \right) \leq \gamma \leq \frac{\epsilon}{2} \left(1 + \sqrt{1 - \frac{1}{\epsilon\omega}} \right). \quad (7)$$

Figure 2 shows the distributions of electrons (positrons) for different s_0 .

4 *A. Eungwanichayapant and F.A. Aharonian*

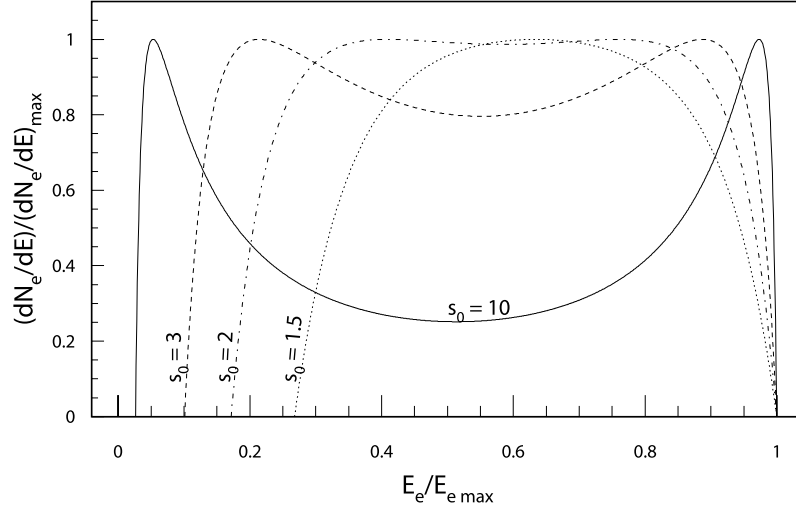


Fig. 2. Differential spectra of electrons and positrons from photon-photon interactions for different values of s_0 : 10 (solid line), 3 (dashed line), 2 (dot-dashed line) and 1.5 (dotted line).

2.2. Inverse Compton scattering

The mean free path of an electron due to the inverse Compton scattering, Λ_{IC} , for the electron propagating through the isotropically distributed photon gas density $n(w)$ is,

$$\Lambda_{IC}^{-1} = \frac{1}{\beta} \int_0^\infty \bar{\sigma}_{IC} n(\omega) d\omega, \quad (8)$$

where the averaged over the angles cross section is

$$\bar{\sigma}_{IC} = \frac{1}{2} \int_{-1}^1 (1 - \beta\mu) \sigma_{IC} d\mu. \quad (9)$$

The total IC cross-section in the lab frame (see e.g. Ref. 16) can be presented in the form

$$\sigma_{IC} = \frac{3\sigma_T}{4\chi} \left[\left(1 - \frac{4}{\chi} - \frac{8}{\chi^2} \right) \ln(1 + \chi) + \frac{1}{2} + \frac{8}{\chi} - \frac{1}{2(1 + \chi)^2} \right], \quad (10)$$

where $\chi = 2w\gamma(1 - \beta\mu)$. The exact solution of Eq.(8) can be presented in an analytical form^{19,20}, but the resulting expression contains a dilogarithm. A quite good approximation, with an accuracy better than 10% has been suggested in Ref. 21.

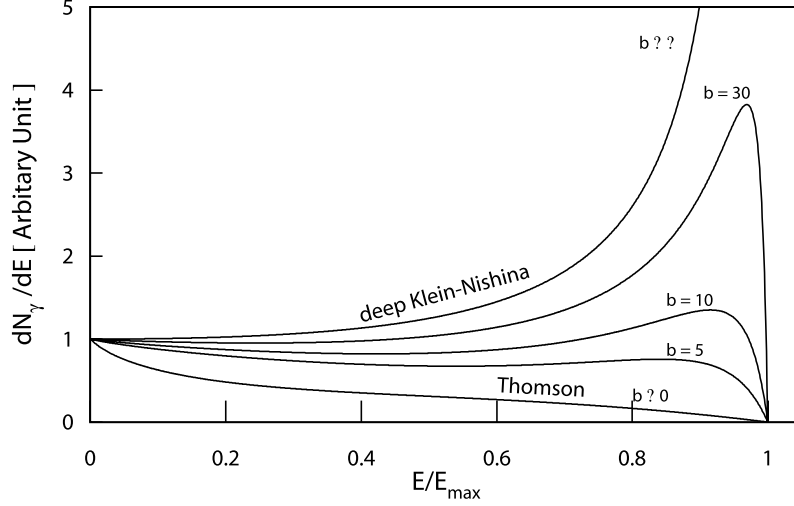


Fig. 3. The spectral energy distribution of upscattered photons (in arbitrary units) for different values of the parameter b : $b \rightarrow 0$, $b = 5$, 10 , 30 , and $b \rightarrow \infty$.

The spectral distribution of the scattered photons via IC for the isotropic photon gas is ²²

$$\frac{dN_\varepsilon}{d\varepsilon} = \frac{3\sigma_T}{4w\gamma^2} \left[1 + \frac{x^2}{2(1-x)} + \frac{x}{b(1-x)} - \frac{2x^2}{b^2(1-x)^2} - \frac{x^3}{2b(1-x)^2} - \frac{2x}{b(1-x)} \ln \frac{b(1-x)}{x} \right], \quad (11)$$

$$\frac{\omega}{\gamma} \ll x \leq \frac{b}{1+b} = \frac{\varepsilon_{max}}{\gamma}; \quad x \equiv \frac{\varepsilon}{\gamma}; \quad b \equiv 4\omega\gamma. \quad (12)$$

The spectra of upscattered photons depend only on the parameter b , as illustrated in Fig. 3. If the value of b is small, as in the Thomson regime, the upscattered photon population is predominantly in the low energy regime. If the value of b is large, corresponding to the Klein-Nishina regime, the population is shifted towards high energies.

3. The method of calculations

In order to study of formation of pair halos and to calculate the characteristics of their radiation, in this work we used the method of Monte Carlo simulations of interactions high energy electrons and photons with intergalactic radiation fields. This method provides an effective tool for study of development of electromagnetic cascades, and, in particular, allows precise calculations of both energy and spatial distributions of cascade particles for an arbitrary background photon field. The method of calculations presented below is described in Ref. 23. For the treatment

of interaction lengths and energy distributions of electrons and photons produced at the photon-photon and electron-photon interactions we used the corresponding total and differential cross-sections of these processes. The hit-or-miss method²⁴ and the rejection method²⁵ have been used for simulations of the interaction lengths and the energy distributions of cascade particles. We assumed that the magnetic field in the intergalactic medium is sufficiently small, so the synchrotron cooling of electrons can be neglected. On the other hand, we assumed that the magnetic field is sufficiently large, thus the secondary electrons of all relevant energies are isotropised before they interact with ambient photons. These two conditions are safely satisfied for a very broad range of the intergalactic magnetic fields between 10^{-7} G to 10^{-12} G.

The background photon fields used in our calculation consist of Cosmic Microwave Background (CMB) and the Extragalactic Background Light (EBL). Both the CMB and EBL are functions of redshift. Since the background photon field at large cosmological redshifts significantly differ from that at the present epoch, the assumption of a consistent background during the development of the cascade cannot be held for the large redshift sources. On the other hand, the cascade simulation with evolving background photon field are computationally expensive. To make calculations faster, the simulation scheme was adjusted by simulating the cascade only at a certain epoch or in the limited region around a source of redshift z_s , when one can assume constant background radiation with the EBL flux corresponding the cosmological epoch of $z = z_s$. Obviously, the simulation region should be big enough to guarantee an adequate accuracy of calculations of the spatial distributions of particles around the central source. At the same time the region should be relatively compact so the constant background approximation can be applied. For example, for a source at a distance of 1 Gpc, the gamma-ray production region around the source with an angular size 5° corresponds to the linear size ≈ 100 Mpc, so we can safely assume that the EBL is not noticeably changed across this size or over the corresponding time of $\leq 3 \times 10^8$ yr.

Beyond the "cascade region", we take into account the interactions with EBL only in terms of absorption (i.e. without of the cascade treatment). Thus the results presented in this paper are relevant only for the core of halos within angular size of a few degree. Although pair halos do extend beyond 5° , their cores, in fact, present the most interest, at least from the point view of detectability of these huge structures. Therefore in most of cases, when we are interested in the compact cores of halos, the calculations are done using this approximate procedure. Within this approach, to calculate the observed energy distribution dN/dE , we modify the distribution dN_{z_s}/dE calculated in the "cascade region" at the epoch z_s , by multiplying to the attenuation factor, $\exp[-\tau_{PP}(\varepsilon)]$:

$$\frac{dN(\varepsilon)}{dE} = \frac{dN_{z_s}(\varepsilon)}{dE} \exp[-\tau_{PP}(\varepsilon)], \quad (13)$$

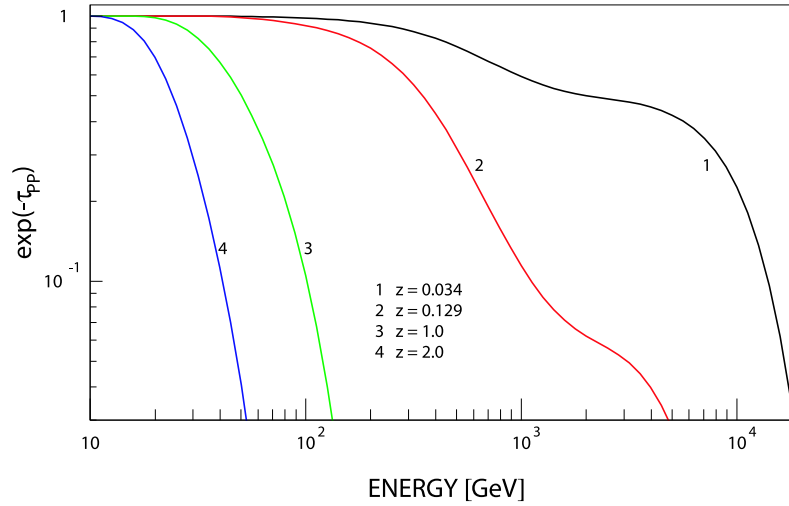


Fig. 4. The attenuation factor $\exp(-\tau_{PP})$ for gamma photons emitted from sources at different redshifts as a function of energy for a specific EBL proposed by Primack et al. (2000).

where τ_{PP} is the PP optical depth,

$$\tau_{PP}(z_s, \varepsilon) = \frac{c}{H_0} \int_0^{z_s} dz (1+z)^{-2} \int_{1/\varepsilon_z}^{\infty} d\omega_z n(\omega_z, z) \bar{\sigma}_{PP}(\varepsilon_z, \omega_z), \quad (14)$$

Here ε_z and ω_z are the γ -ray and background photon energies at the redshift z , H_0 is the Hubble constant; in this paper we use $H_0 = 65$ km/s/Mpc. The attenuation factors at different redshifts are shown in Fig. 4.

4. Results

Below we present results of calculations of the spectral energy distributions (SEDs) and angular distributions of gamma-rays from pair halos around sources located at different redshifts. The main uncertainty of predicted energy spectra and morphology of pair halos is related to the uncertainties of EBL, especially in the mid and far infrared wavelengths. Here we use three different EBL models proposed by Malkan & Stecker (1998, hereafter M98)⁵, Primack et al. (2000, hereafter P00)⁶ and Kneiske et al. (2002, hereafter K02)⁷. One should note the recent developments related to the EBL at near infrared and optical wavelengths (see e.g. Ref. 8, 9). However this wavelength band is not critical for formation of pair halos. On the other hand the above models represent quite broadly the possible range of EBL at most principal (from mid- to far- infrared) bands responsible for formation of pair halos around sources with redshifts up to $z \sim 2$.

In Fig. 5 we present the Spectral Energy Distribution (SED) of a pair halo within different angles formed around a source with redshift $z_s = 0.129$. This cor-

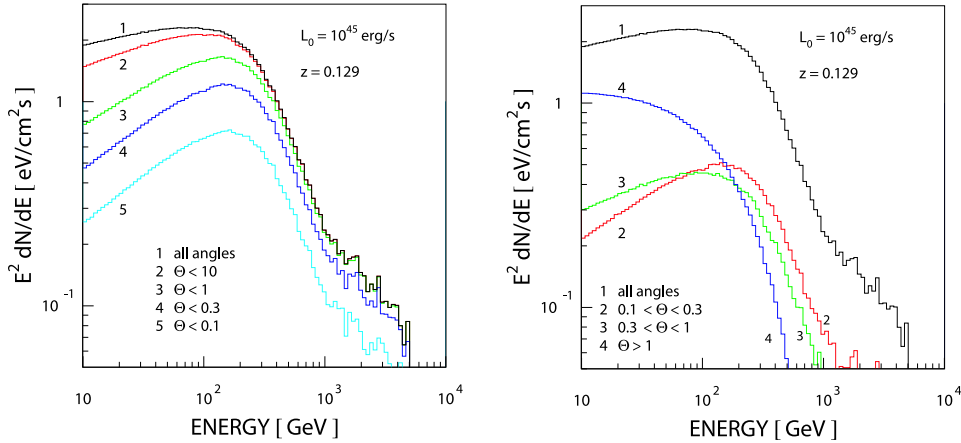


Fig. 5. The SED of a pair halo at $z = 0.129$ within $\Theta \leq 10^\circ$, 1° , 0.3° , and 0.1° (left panel) and $0.1^\circ \leq \Theta \leq 0.3^\circ$, $0.3^\circ \leq \Theta \leq 1^\circ$, and $\Theta \geq 1^\circ$ (right panel). In both panels the SEDs integrated over all angles are also shown.

responds to the redshift of the blazar 1ES 1426+482, but is also representative for many TeV blazars reported by the HESS, MAGIC and VERITAS collaborations. For the EBL we adopted the P00 model. The calculations are performed for a monoenergetic spectrum of primary gamma-rays with $E_0 = 100$ TeV and luminosity $L_0 = 10^{45}$ erg/s.

The differential angular distribution of gamma-ray flux of the pair halo in different energy bands is shown in Fig. 6 (left panel). The angular distribution of the cumulative flux, $J_\gamma(\geq \Theta^2)/J_\gamma(\text{all angles})$ is shown in Fig. 6 (right panel). The initial parameters are the same as in Fig. 5. As expected at higher energies the halo looks more compact than at lower energies. This is clearly seen also in Fig. 7, where the two-dimensional projections of pair halos at different energies are shown.

4.1. *The impact of the initial gamma-ray spectrum*

In order to study the impact of the initial gamma-ray spectrum on the basic characteristics of pair halos, we calculated the angular and spectral distributions of gamma-rays for a halo initiated by monoenergetic gamma-rays. The results are shown in Fig. 8 for three different energies of primary gamma-rays: $E_0 = 20$, 100, and 500 TeV. One can see that at the intermediate (around the maximum of SED) and low energies both the energy and angular distributions are quite insensitive to the primary energy. The latter becomes important at higher energies, namely between 1 TeV and 10 TeV. In particular, with an increase of E_0 the angular distribution becomes sharper, especially below 0.1° . Also, with an increase of E_0 , the energy spectrum beyond the maximum around a 100-300 GeV becomes significantly flatter. This tendency continues, however, until $E_0 \sim 100$ TeV. At higher energies

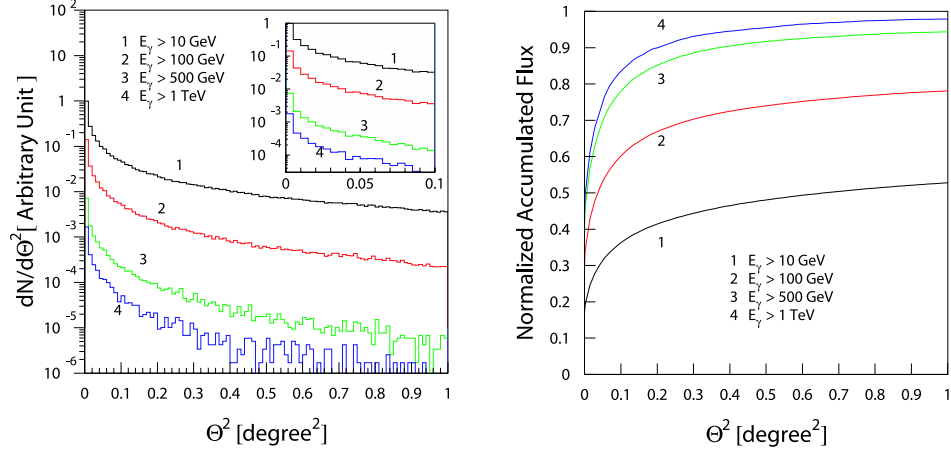


Fig. 6. Left panel: differential angular distributions of the pair halo at $z = 0.129$ (in arbitrary units); Right panel: cumulative angular distributions at different energies.

of primary gamma-rays, the results of the spectral and angular distributions of the halo radiation becomes almost insensitive to E_0 .

4.1.1. Power law sources

In Fig. 9 we show the energy and angular distributions of radiation of the pair halo for more realistic, power-law distribution of primary gamma-rays, $Q(E) \propto E^{-\Gamma}$ between 100 GeV and 100 TeV, and $Q(E) = 0$ outside this interval. The results calculated for three different values of $\Gamma=1, 1.5$, and 2, but for the fixed total gamma-ray luminosity $L_0 = 10^{45}$ erg/s are shown in Fig. 10. The results are quite similar which is explained by the fact that for the chosen hard energy spectra of primary gamma-ray, the main contributions come from the energy interval close to $E_{\text{max}} = 100$ TeV.

In Fig. 10 we show the case of primary gamma-rays with fixed power-law photon

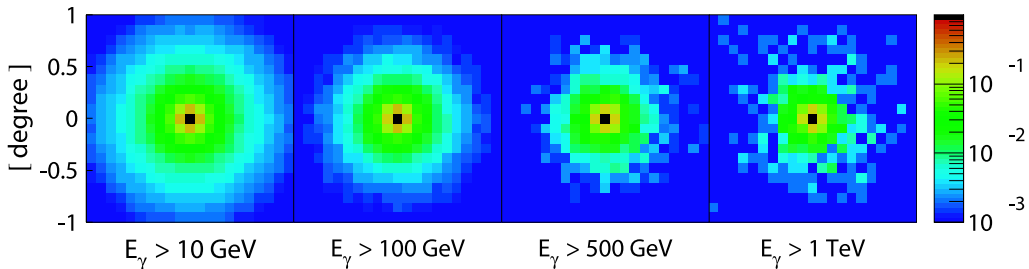


Fig. 7. Two dimensional map of a pair halo at $z = 0.129$ at different gamma-ray energies.

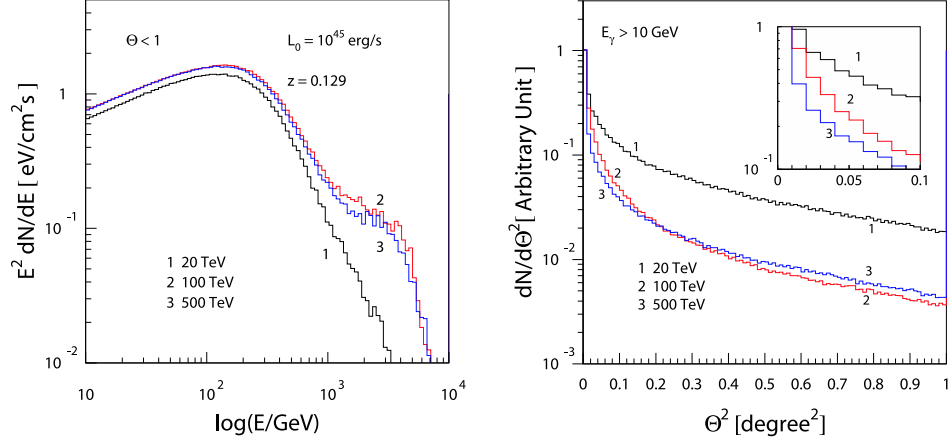
10 *A. Eungwanichayapant and F.A. Aharonian*


Fig. 8. Radiation of pair halos initiated by monoenergetic gamma-rays with $E_0 = 20, 100$ and 500 TeV. Left panel: SEDs; Right panel: angular distributions.

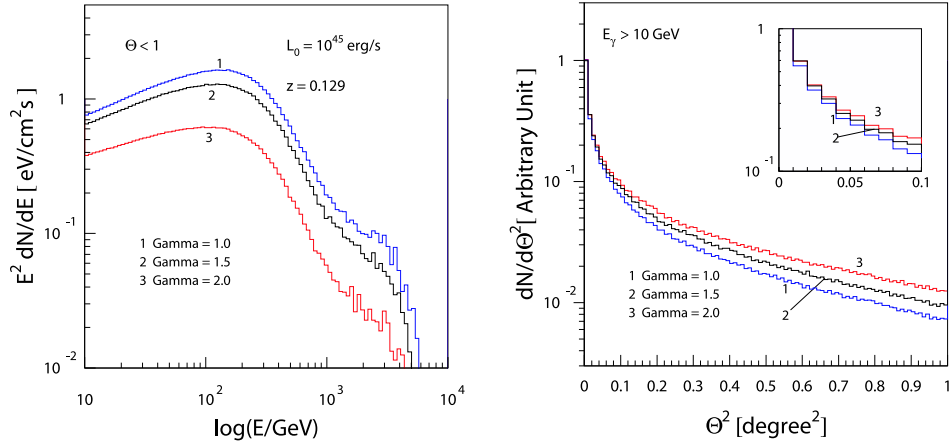


Fig. 9. Pair halos initiated by primary gamma-rays with power-law spectrum between $E_{\min} = 100$ GeV and $E_{\max} = 100$ TeV for different photon indices $\Gamma=1, 1.5,$ and 2 . Left Panel - SED; Right Panel - angular distribution.

index $\Gamma = 1.5$, and for different maximum energies, $E_{\max} = 10, 30, 100$ TeV. It is interesting that the pair halo SEDs are more sensitive to E_{\max} between 10 to 30 TeV, whereas the angular distributions are more sensitive to E_{\max} between 30 to 100 TeV.

4.2. Redshift Dependence

When the redshift of the source exceeds 0.1 one has to take into account the evolution of EBL in the past. The energy density of the CMB increases with z propor-

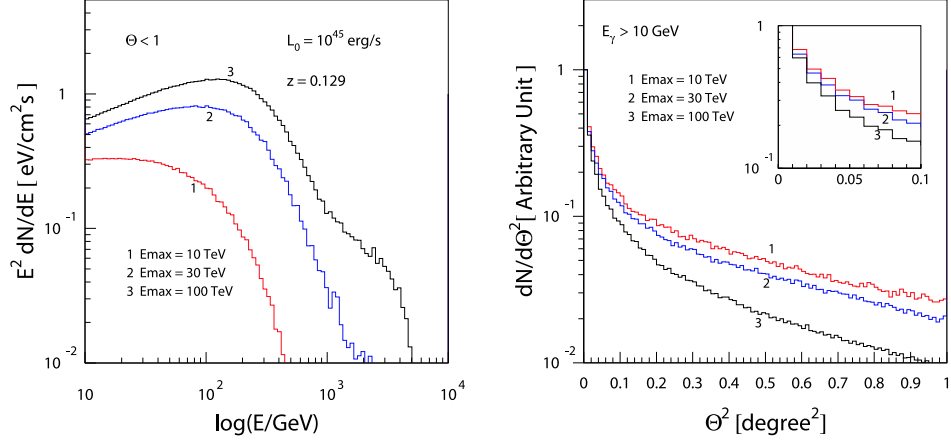


Fig. 10. Pair halos calculated for a power-law spectrum of primary gamma-rays with $\Gamma=1.5$ and three different $E_{\max}=10$ TeV, 30 TeV, and 100 TeV. Left panel- SEDs, Right panel - angular distributions.

tional to $(1+z)^4$, while the peak of distribution shifts to higher energies by a factor of $(1+z)$ (see Fig 11). The EBL evolution is different from the CMB evolution since both the stellar-light and the dust component of EBL are produced at much later epochs with $z \lesssim 3$.

In Fig. 11 we show the evolution of EBL, i.e. the EBL flux at different epochs z in accordance with the P00 model (left panel). The corresponding mean free paths are shown in the right panel of Fig. 11. One can see that at the epoch $z = 2$, the

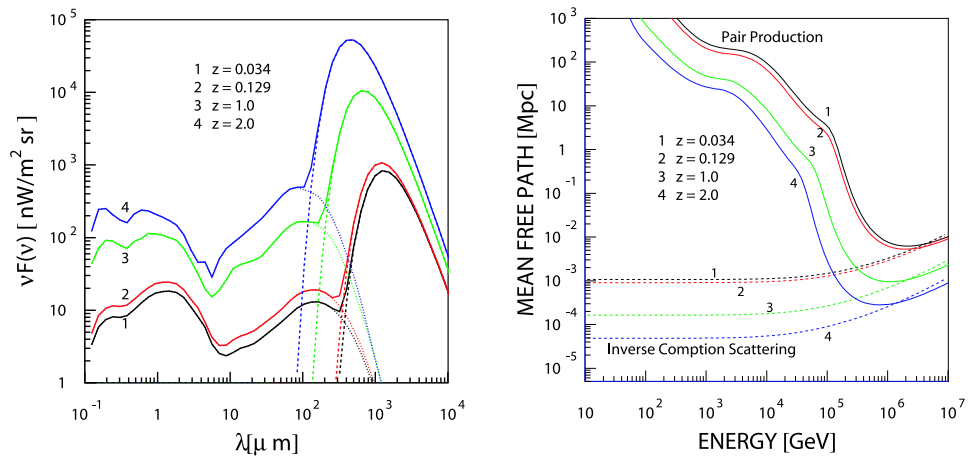


Fig. 11. Left panel: EBL at different redshifts; Right panel: mean free paths of gamma-rays due to pair production (PP) and electrons due to the inverse Compton (IC) scattering at different epochs.

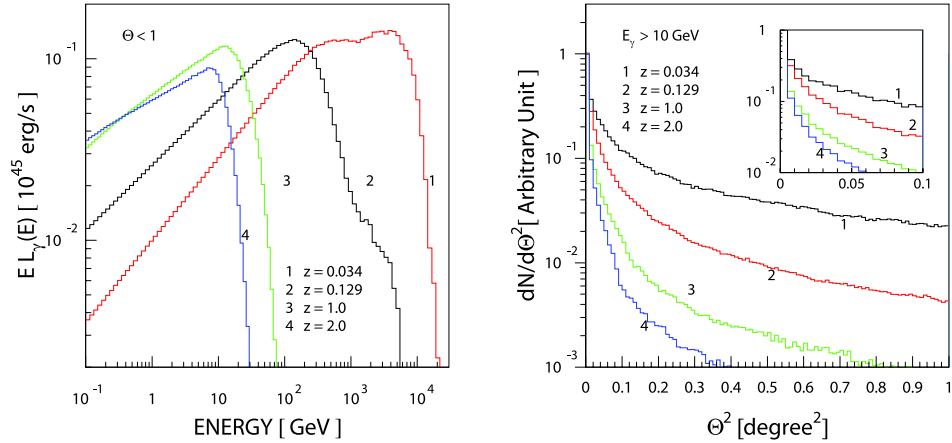


Fig. 12. Spectral luminosities of pair halos calculated for sources located at different redshifts, $z = 0.034, 0.129, 1$ and 2 , for the opening angle 1° (left panel). Angular distributions of gamma-rays at energies above 10 GeV (right panel).

mean free paths of gamma-rays and electrons in the intergalactic medium were an order of magnitude shorter than at the present epoch. This should obviously result in significant shift of the SED towards low energies and more compact halos (in addition to the effects introduced by the redshift itself). This is demonstrated in Fig. 12, where the spectral luminosities and angular distributions of radiation of pair halos are shown for different redshifts of central sources. The total luminosity of primary gamma-rays is assumed 10^{45} erg/s.

4.3. Dependence on the EBL models

For energy spectrum of primary gamma-rays extended to $E \leq 10^3$ TeV, the e^\pm pairs are produced mainly through interactions with the EBL photons. Therefore, the choice of the EBL model is principal for calculations of characteristics of pair halos. To study the impact of the EBL on the pair halos, we calculated the parameters of pair halos for two different EBL models. The EBL from P00 is based on semi-analytic calculations. All physical processes, including the formation and evolution of galaxies are included in the code. The EBL model M98 is based on empirical assumptions. It adopts an EBL flux at the present epoch ($z = 0$), and assumes time evolution proportional to $(1 + z)^{3.1}$. These two EBL models for $z = 0.129$, as well as the corresponding mean free paths of gamma-rays are shown in Fig. 13.

In Fig. 14 we show the SEDs and angular distributions of a pair halo located at $z = 0.129$ calculated for two EBL models shown in Fig. 13. One can see that while the SEDs are quite similar at low energies, the energy spectrum corresponding to the P00 model is significantly shifted compared to the SED predicted by the M98 EBL model. Also, the P00 EBL model predicts sharper angular distribution, especially at

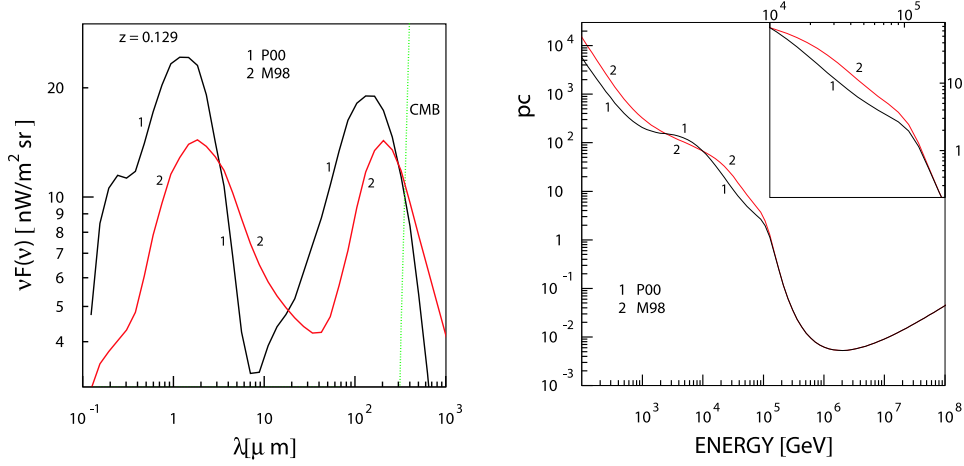


Fig. 13. Left panel: Spectral energy distributions of the P00 and M98 EBL models at the present epoch, $z = 0$; Right panel: the mean free paths of gamma-rays for these two models, respectively.

$\geq 0.1^\circ$. This is explained by the higher EBL flux at mid and far-infrared wavelengths assumed in the P00 model.

For sources with large redshifts, $z \gg 0.1$, the energy and angular distributions of pair halos depends on the time-evolution of EBL. In fact, this dependence is stronger than the dependence on the EBL flux at the present epoch. To demonstrate this effect, in Fig. 15 we show the spectral and angular distributions of a halo at $z = 2$ calculated for two EBL models - P00 and K02⁷, which are characterised

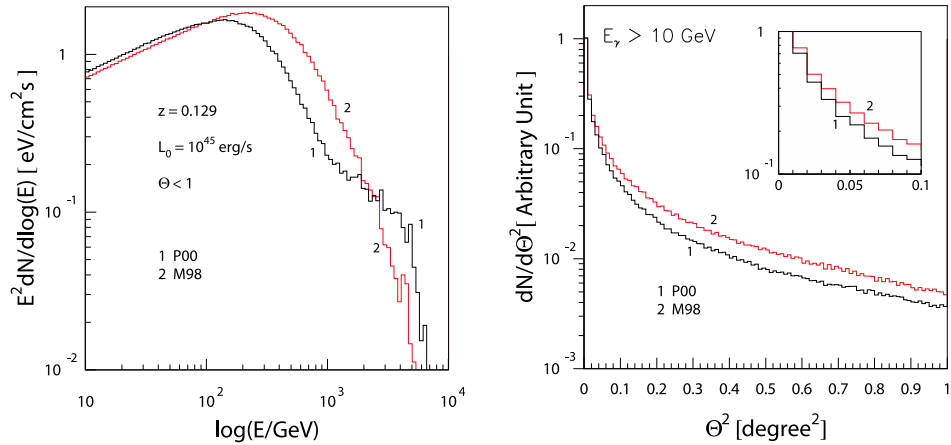


Fig. 14. Left panel: differential angular distributions of radiation of a pair halo at $z = 0.129$ calculated for the P00 and M98 models; Right panel: cumulative angular distributions.

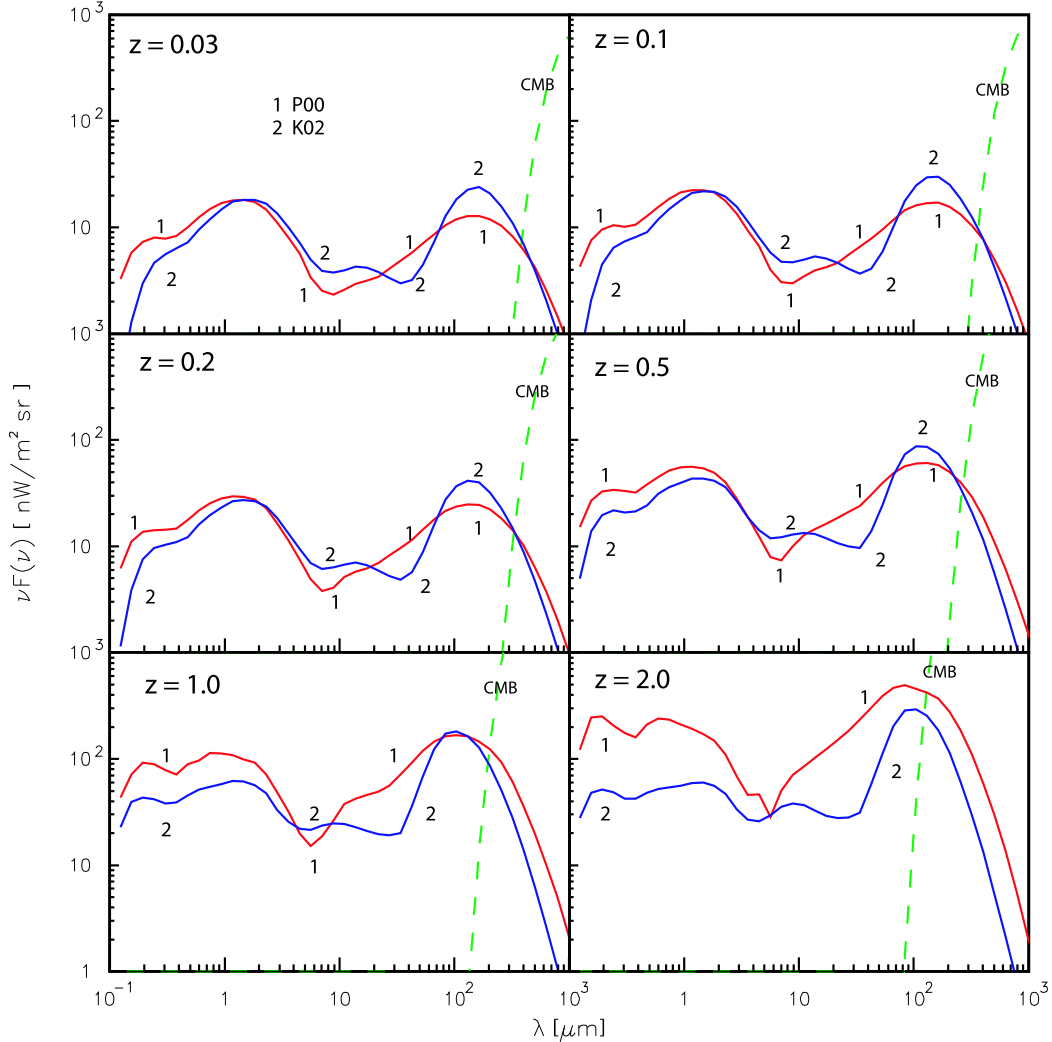


Fig. 15. The EBL fluxes at different redshifts predicted by the P00 and K02 models.

by significantly different cosmological evolution of the EBL flux. These two models predict relatively similar fluxes at present epoch (or at low redshifts, $z \leq 0.1$). However, at large cosmological epochs, $z \geq 1$, the difference of two models becomes as large as an order of magnitude. This is seen in Fig. 15, where the EBL fluxes predicted by the P00 and K02 model are shown for six different cosmological epochs. The corresponding SEDs and differential angular distributions are shown Fig. 16 and 17. One can see that while at low redshifts two EBL models give relatively similar spectral and angular distributions of gamma-rays, at $z = 2$ the difference in predictions of two EBL models becomes significant.

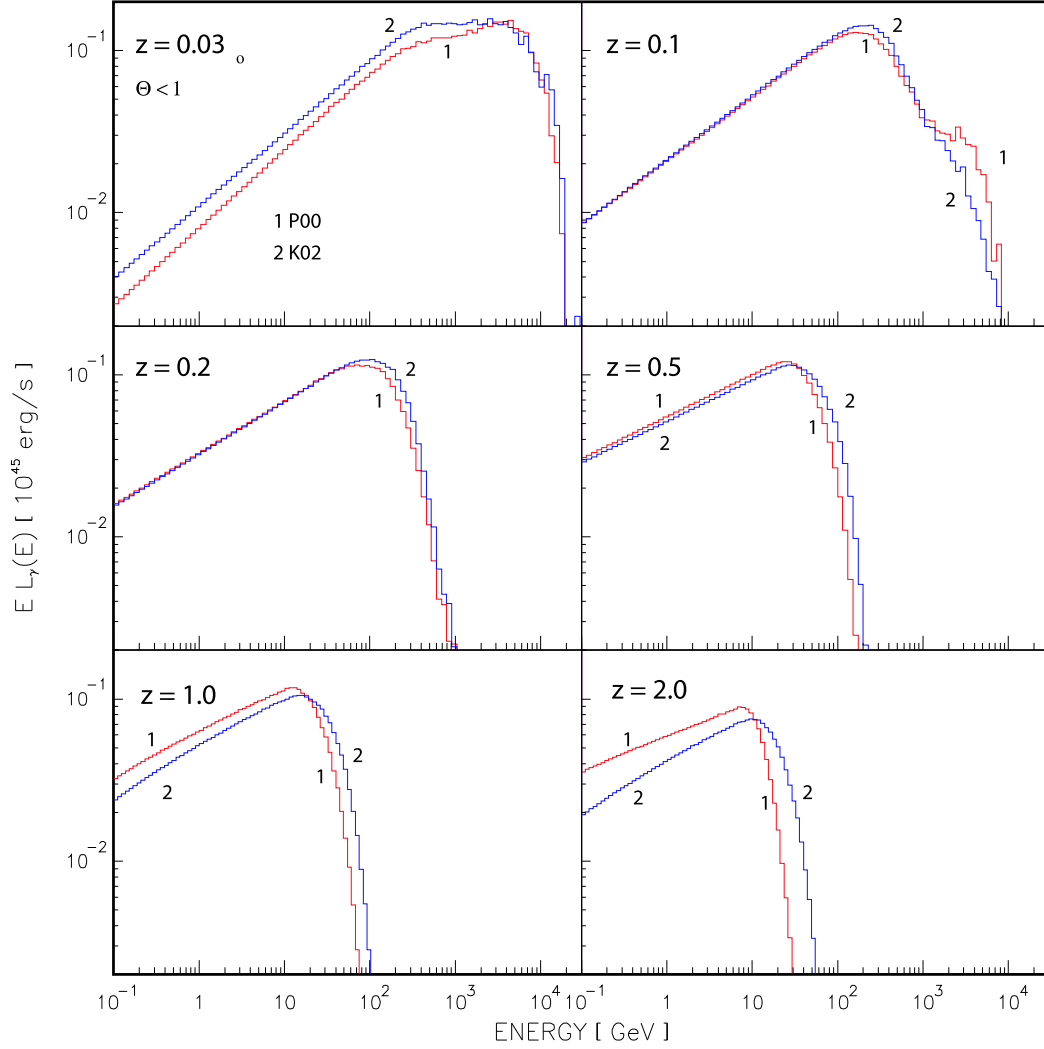


Fig. 16. Spectral luminosity distributions of the pair halos corresponding to each EBL models

5. Summary

Interactions of high energy gamma-rays with EBL initiate electromagnetic cascades which lead to formation of electron-positron halos around powerful nonthermal extragalactic sources. The pair halos contain unique information about the flux of EBL and its time-evolution in the past. We studied the dependence of radiation of pair halos on several key parameters, in particular on the energy spectrum of the primary gamma-rays, the source redshift, and the EBL flux. The results presented in this paper can be used for search for these giant structures which can serve as

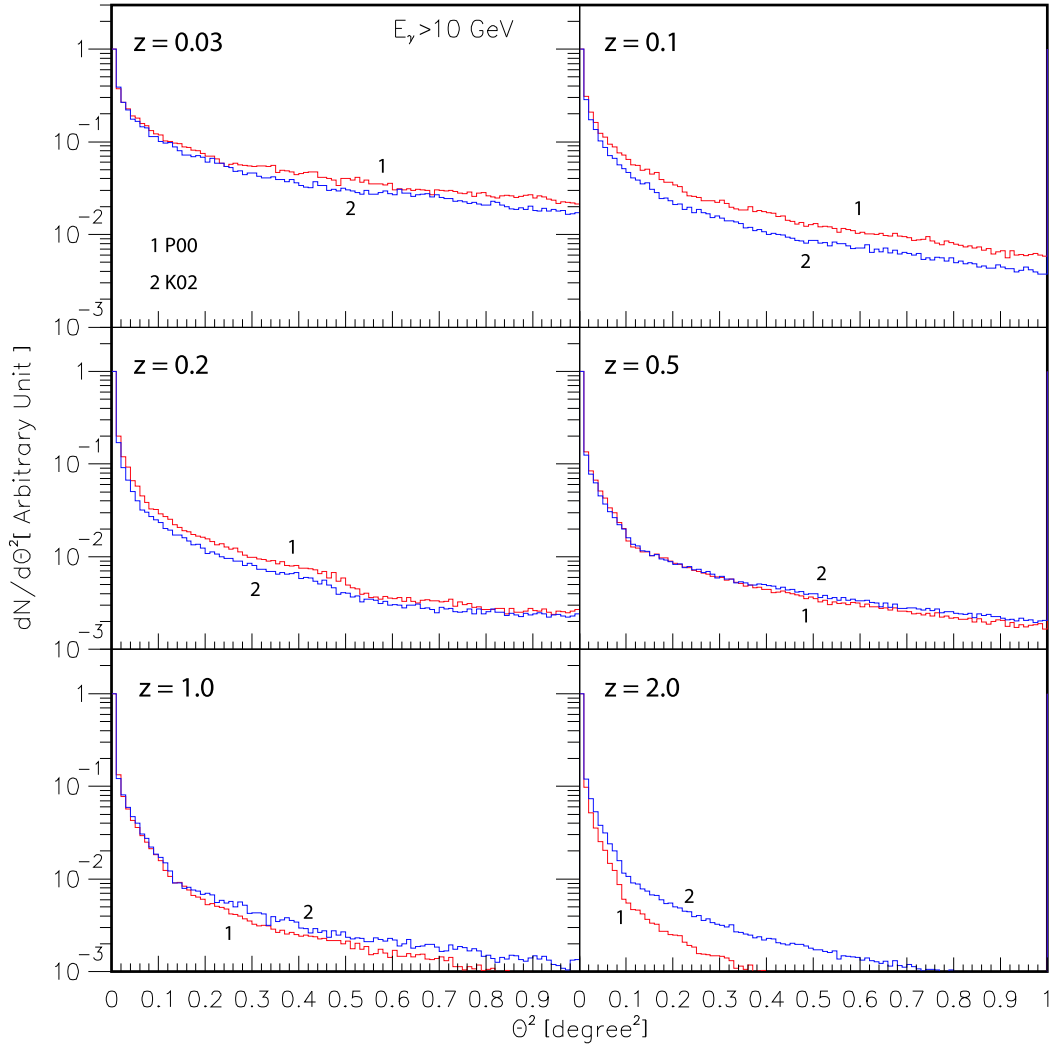


Fig. 17.

unique cosmological candles.

References

1. A.I. Nikishov, *Sov. Phys. JETP* **14** (1962) 393.
2. R. J. Gould and G. Schröder, *Phys. Rev.* **155** (1967) 1408.
3. F.A. Aharonian, A.N. Timokhin, A.V. Plyasheshnikov, *A&A* **384** (2002) 834.
4. E.Dwek and J. Slavin, *ApJ* **436** (1994) 696.
5. M. A. Malkan and F. W. Stecker, *ApJ* **496** (1998) 13.
6. J. R. Primack, R. S. Somerville, J. S. Bullock, and J. E. G. Devriendt, in *Proc. High*

- Energy Gamma-Ray Astronomy Int. Symp.*, eds. F. A. Aharonian and H. J. Völk (Melville, New York, 2001), p. 463.
7. T. M. Kneiske, K. Mannheim, and D. H. Hartmann, *A&A* **386** (2002) 1.
 8. A. Franceschini, G. Rodighiero, M. Vaccari, to appear in *A&A* (2008).
 9. J. Primack, to appear in *Proc. High Energy Gamma-Ray Astronomy Int. Symp.*, eds. F. A. Aharonian et al. (Melville, New York, 2009).
 10. F. A. Aharonian, TeV Blazars and cosmic infrared background radiation, in *Invited, Rapporteur, and Highlight Papers. Proc. 27th Int. Cosmic Ray Conf. Highlight papers*, eds R. Schlickeiser (2001), Hamburg, p. 250.
 11. P.S. Coppi and F.A. Aharonian, *ApJ* **521** (1999) L33.
 12. B. McBreen, *A&A* **71** (1979) L19.
 13. F.A. Aharonian, D. Khangulyan, L. Costamante, *MNRAS* **387** (2008) 1206.
 14. A. Reimer, *ApJ* **665** (2007) 1203.
 15. F.A. Aharonian, P.S. Coppi, H.J. Völk, *ApJ* **423** (1994) L5.
 16. A. I. Akhiezer and V. B. Berestetskii (eds.), *Quantum Electrodynamics*, (Interscience Publishers, New York, 1965).
 17. F. A. Aharonian (ed.), *Very High Energy Cosmic Gamma Radiation: A Crucial Window on the Extreme Universe*, 1st edn. (World Scientific, Singapore, 2004).
 18. F. A. Aharonian, A. M. Atoyan, and A. M. Nagapetian, *Astrofizika* **19** (1983) 187.
 19. F. A. Aharonian, V. G. Kirillov-Ugryumov, and V. V. Vardanian, *Astrophys. Space Sci.* **115** (1985) 201.
 20. R. J. Protheroe, *MNRAS* **221** (1986) 769.
 21. P. S. Coppi and R. D. Blandford, *MNRAS* **245** (1990) 453.
 22. G. R. Blumenthal and R. J. Gould, *Rev. Mod. Phys.* **42** (1970) 237.
 23. A. Eungwanichayapant, PhD thesis, University of Heidelberg, 2003.
 24. F. James, *Rep. Prog. Phys.* **43** (1980) 1145.
 25. W. H. Press, S. A. Teukolsky, W. T. Vetterling, and B. P. Flannery, *Numerical Recipes in C*, 2nd edn. (Cambridge university press, New York, 1994).